



HAL
open science

Robot guidance of an ultrasound probe toward a 3D region of interest detected through X-ray mammography

Marie-Aude Vitrani, Anja Marx, Razvan Iordache, Serge Muller, Guillaume Morel

► To cite this version:

Marie-Aude Vitrani, Anja Marx, Razvan Iordache, Serge Muller, Guillaume Morel. Robot guidance of an ultrasound probe toward a 3D region of interest detected through X-ray mammography. International Journal of Computer Assisted Radiology and Surgery, 2015, pp.1861-6429. 10.1007/s11548-015-1244-8 . hal-01170661

HAL Id: hal-01170661

<https://hal.science/hal-01170661v1>

Submitted on 2 Jul 2015

HAL is a multi-disciplinary open access archive for the deposit and dissemination of scientific research documents, whether they are published or not. The documents may come from teaching and research institutions in France or abroad, or from public or private research centers.

L'archive ouverte pluridisciplinaire **HAL**, est destinée au dépôt et à la diffusion de documents scientifiques de niveau recherche, publiés ou non, émanant des établissements d'enseignement et de recherche français ou étrangers, des laboratoires publics ou privés.

Robot guidance of an ultrasound probe towards a 3D region of interest detected through x-ray mammography

Marie-Aude Vitrani · Anja Marx · Răzvan Iordache · Serge Muller · Guillaume Morel

Received: date / Accepted: date

Abstract *Purpose:* This research is situated in the context of breast cancer detection where the standard procedure is the succession of an initial mammography (MX) examination and a supplementary Ultrasound (US) scan. One major difficulty of this procedure results from the fact that breast geometry changes between both examinations due to different patient's positions. The proposed system facilitates this combined examination by keeping the breast geometry and by adding a US probe guidance robot to the mammography system.

Methods: A co-manipulation system is set up where the robot and user simultaneously manipulate the probe towards the target previously localized in MX images. Calibration procedures and robot control are detailed.

Results: A test protocol was presented to conduct two tests that are both related to the medical application. The first tests aims at evaluating robot guidance for localizing a lesion which was previously defined in the X-ray images. The second tests aims at quantifying robot influence when scanning a target lesion. The studied task consists of a pointing/scanning exercise, where the US beam intersects a breast lesion.

Conclusions: The experiments show a significant increase in examination quality when using robot guidance as compared to the non-assisted examination.

Keywords comanipulation · human-robot collaboration · breast cancer detection · assisted gesture

1 Introduction

This work is set in the medical context of breast cancer (BC) detection. The usual BC detection procedure schedules a first x-ray examination (called mammography

A. Marx, M.-A. Vitrani and G. Morel are with (1) Sorbonne Universités UPMC Univ. Paris 06, UMR 7222, ISIR, Paris, France, (2) INSERM, U1150, Agathe-ISIR, F-75005, Paris France, (3) CNRS, UMR 7222, ISIR, F-75005, Paris, France. Email: {marx, vitrani, morel}@isir.upmc.fr · A. Marx, R. Iordache and S. Muller are with GE Healthcare, Buc, France.

(MX), Fig.1) followed by a supplementary MX plus Ultrasound (US) examination if necessary, Fig.2.



Fig. 1 MX examination

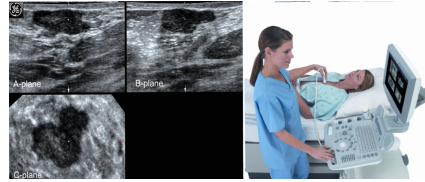


Fig. 2 US examination

MX and US are both used because they represent complementary modalities in breast imaging. MX has proven to be very effective detecting early cancers in mostly adipose breasts, while US is more sensitive in dense breasts. For dense breasts, tissue characteristics sometimes prohibit accurate BC identification. As a result, about half of cancers with histological confirmation were missed using MX during a study on patients with dense breasts [1]. Meanwhile, attempting BC detection in women having dense breasts remains essential as 50% appx. of young women have such breasts [9]. Furthermore, BC risk increases by a factor of 4 to 6 for women having dense breasts [12]. US is thus used in combination with MX as it has been reported, to be more sensitive than MX for BC detection in dense breasts, [5], [15], [11], [17], [13]. Therefore, combining MX and US into a single examination has the potential to provide an effective tool for BC diagnosis in women with dense breasts.

One of the main problems in conducting MX followed by manual US is the change of breast geometry. Indeed in MX, the breast is compressed between the image receptor and a compression paddle before x-ray exposure. On the other hand, for US, the patient is lying on her back and the breasts are not compressed anymore. The examiner has to mentally correlate the suspicious zone identified in the MX images with the new geometry of the uncompressed breasts. Conway *et al.* reported in their study [6], that examiners fail to locate up to 10% of the lesions during manual US: in 10% of manual US following MX, the examiner was going to investigate a different breast lesion than the one previously seen in MX and was not aware of the mismatch.



Fig. 3 Semi-automated US breast scanning system, [14].

To overcome these difficulties, Kapur *et al.* proposed an imaging apparatus to combine MX and automated US scans [14], see Fig.3. A 2 degrees of freedom (DOFs) robotized probe holding framework is mounted on top of the compression paddle. During the US examination, the probe is automatically moved over the compression paddle and the images are further treated in order to display the scanned US volume. MX and US images are displayed in real time. Since US coupling gel might have a negative affect on MX image quality, MX is performed prior to US. A clear advantage of this approach is that the patient's breast remains under the same compression during MX and US. A drawback in the context of diagnostic procedures is that it may take time to fully scan the breast volume with the US probe, while the medical need is often to check a particular suspicious region that was detected on MX. Moreover, when shadows appear from either anatomical structures or paddle support, it is not possible to adapt the probe's orientation because of the limited DOFs of the scanning device.

The concept developed in this paper uses the same idea of performing the US examination right after the MX imaging, the patient's breast remaining under the same compression. However, instead of an automatic scanning with limited number of DOFs, we propose a manual manipulation of the US probe towards a target localized in the MX image, with six DOFs. This manipulation is assisted by a comanipulated system.

Comanipulation consists in sharing the control of a tool between a user and a robot. A typical behavior is set through *Virtual Fixtures*. Virtual fixtures are geometrical constraints imposed by a robot to a tool: along some DOFs, the movement is free for the user while along the others, it is blocked up to the robot programmable stiffness.

This idea was implemented in [20] and [19], through a semi-passive device called Passive Arm with Dynamic Constraints (PADyC). Its mechanical design enables the motion of a tool to be limited in accordance with a planned task. A geometric zone is defined in which the surgeon can move freely. When moving out of the zone the surgeon is restricted by forces applied by the robot, which prevents the tool from leaving the prescribed zone. Since then, comanipulation and virtual fixtures have been widely used for surgical applications ranging from orthopedic surgery, [7], [3], [10] to eye surgery [16], through key-hole interventions, [18]. The application of comanipulation to the placement of an US probe following an MX exam for BC detection is detailed in Sec.2. This application requires a full system calibration, which is described in Sec.3 and an original controller described in Sec.4. A set of in vitro experimental results is given and discussed in Sec.5 prior to a conclusion (Sec.6).

2 Proposed approach

The workflow of the proposed system begins with a 3D Mammography so-called Digital Breast Tomosynthesis (DBT) scan of the patient's breast, see Fig.4. After 3D reconstruction of the breast a suspicious zone is identified. Its coordinates are sent to the robot in order to provide assistance when locating the target lesion. The user jointly manipulates the probe with the robot. His/her task is to image the suspicious

zone while maintaining contact between the probe and the paddle. The robot task is to

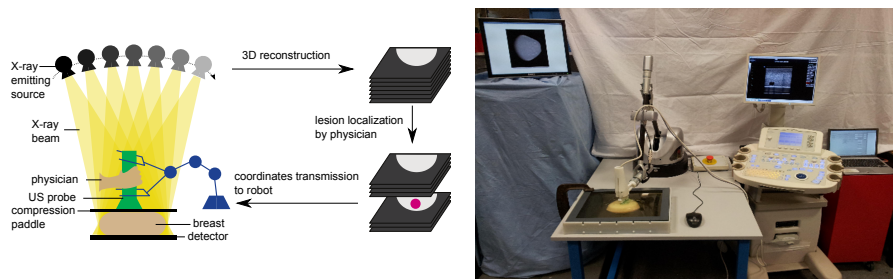
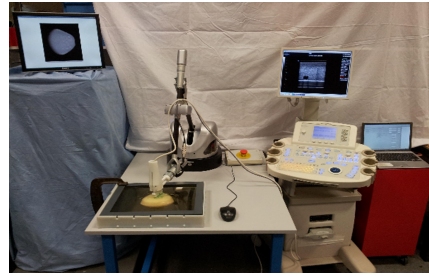


Fig. 4 Novel system for robot assistance for combining US and DBT examinations. **Fig. 5** Test Setup



help the radiologist thanks to virtual fixtures, see Fig.4. Indeed, from the physician's point of view the US scan remains complex: to position the probe, the shape and 3D-location of the suspicious lesion must still be mentally reconstructed from the DBT images. This computation can be performed easily by a computer and the information can then be sent to a robot, which should guide the physician towards the lesion with increased speed and accuracy. Fig. 5 depicts the complete setup built to experiment this idea. A Virtuose 6D (Haption, France) robot is used. It is a fully actuated 6-DOFs haptic robot which is designed to produce forces and moments at its end-effector with a high fidelity. Adaptable fixations were built to mount on the robot end-effector a 9L linear transducer (Ultrasonix, France) connected to an Ultrasonix RP Ultrasound system.

As for the breast, a multi modal breast phantom (Cirs inc. model 051 phantom) containing dense masses of 2 to 8 mm diameter and cystic lesions of 3 to 10 mm diameter is used. It is compressed between a 25 mm thick PVC plate (at the bottom) and a 6 mm thick PMP plate (at the top), both well suited regarding their low x-ray attenuation, PMP being equally well suited to let pass US [4]. Figure 6 show typical US-image of a lesion obtained with this set-up. A computer screen is placed in front of the subject and displays the reconstructed slices of the breast phantom, acquired using an investigational DBT device based on a Senographe DS (GE Healthcare, Chalfont St Giles, UK). The subjects are free to navigate within the DBT images using the scroll ball of a computer mouse, as it is done during the standard workflow of mammography image reading.

3 System calibration

The proposed approach leads to calibration and registration issues. The target I is first identified in the MX images. Its position in the breast phantom is thus known w.r.t. the x-ray DBT reconstructed slices. The aim is to program the robot assisting the positioning of the probe towards the target. Therefore, it is required to determine

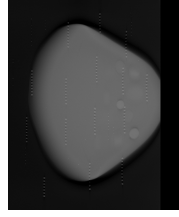
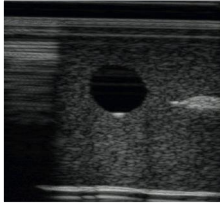


Fig. 6 US image during tests. Left: breast border, **Fig. 7** X-ray image during tests. Top: artifacts due to compression paddle, Bottom: artifacts due to plate simulating the detector, Middle: cystic lesion (black) and tumor lesion (white)

the position of I w.r.t. the ultrasound probe. Two essential localization information are necessary:

- the US-beam localization in robot base (Fig. 8), expressed through the homogeneous translation matrix M_{0P} , resulting from the product of:
 - the robot end effector localization w.r.t. the robot base, M_{06} , (calibration detailed in Sec.3.1),
 - and the US-beam localization w.r.t. the robot end-effector, M_{6P} , (calibration detailed in Sec.3.2),
- the x-ray image frame localization w.r.t. the robot base, M_{0X} , (Fig. 9), (registration detailed in Sec.3.3).

In the next, the following coordinate frames will be used:

- $\mathcal{F}_P = (P, \mathbf{x}_P, \mathbf{y}_P, \mathbf{z}_P)$, the frame attached to US-probe, with P being the probe tip and \mathbf{z}_P the normal vector of the US-plane. Note that $(P, \mathbf{x}_P, \mathbf{y}_P)$ is the US image-plane.
- $\mathcal{F}_0 = (O_0, \mathbf{x}_0, \mathbf{y}_0, \mathbf{z}_0)$, the frame attached to the robot base.
- $\mathcal{F}_6 = \{O_6, \mathbf{x}_6, \mathbf{y}_6, \mathbf{z}_6\}$ the coordinate system of the robot end-effector.
- $\mathcal{F}_X = \{O_X, \mathbf{x}_X, \mathbf{y}_X, \mathbf{z}_X\}$ the coordinate system of the x-ray DBT reconstructed slices, with O_X being the upper left image corner and \mathbf{z}_X the image's normal vector.

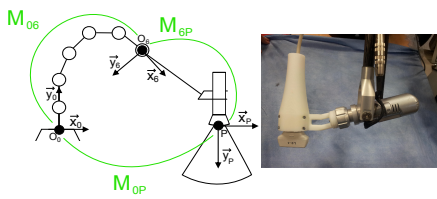


Fig. 8 Ultrasound probe to robot base calibration principle.

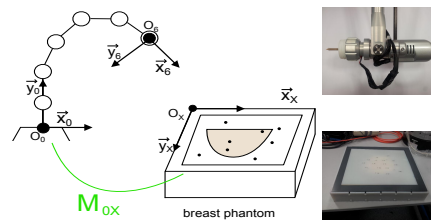


Fig. 9 x-ray image to robot base registration principle.

3.1 Robot Identification

In this system, a cable-driven robot is used. This type of robot may show internal position errors due to their mechanical structure (cable deformations). To interpret the calibration and registration results in their given context, the precision of the robot was determined first. A conventional geometry calibration procedure was run, leading to the identification of the Denavit-Hartenberg (DH) parameters for the Virtuose 6D [8]. DH parameters correspond to the geometrical constants of the robot (link lengths, angles between axes).

The identification consists in minimizing (with an iterative least-square algorithm) the error between two measures of the position of a given end-effector point M . The first measure is obtained from the robot joint sensors and a geometrical model involving the DH parameters to be identified. The second measure is obtained from an external reference measure. In these experiments, the Polaris visual tracking system (Northern Digital Inc.) with a known position error noise of 0.4 mm was used for reference measures, while a visual marker was fixed at the robot end-effector (point M). The robot was positioned in different configurations and the robot and markers positions are recorded in both systems respectively (i.e. Virtuose 6D and Polaris). A total of 37 measures have been used for the identification. The mean end-effector position error after convergence was 1.64 mm (max 2.65 mm, std dev 0.64 mm). The optimized parameters were verified with 13 points not used for optimization, giving an average error of 1.49 mm (max 2.64 mm, std dev 0.81 mm).

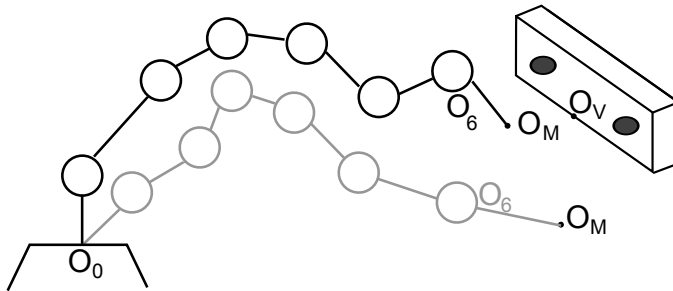


Fig. 10 Verification results of the DH identification algorithm for the Virtuose 6D robot.

3.2 Ultrasound Probe To Robot End Effector Localization

Calibrating the US-probe with respect to the robot end-effector aims at localizing every US image pixel in the robot end-effector frame, i.e. determining the transformation matrix M_{6P} between \mathcal{F}_6 and \mathcal{F}_P . The approach depicted in [21] is used: a rectilinear rod plunged in a water tank is observed by the US probe for several robot

configurations (see Fig.11). The intersection of the calibration rod with the US-plane results in a white blob in a mostly black US image and thus its geometrical center (GC) can easily be localized in the US image. The identification procedure consists

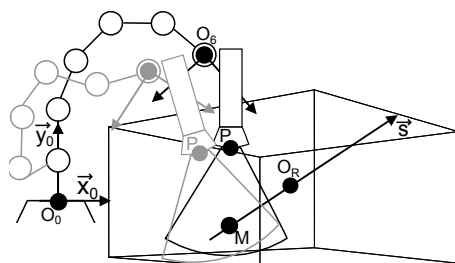


Fig. 11 Geometrical Model For US-Probe Calibration.

in minimizing (thanks to a recursive least square algorithm) the error between two different measures of the GC coordinates in the end-effector frame. One results from the geometrical model of the robot and the other from image processing. Note that the identification procedure also allows for identifying the US image gains, namely the mm to pixel ratio, see [21]. The calibration algorithm is ran from 16 configurations. It converges with an average error of 1.17 mm (max 2.41 mm, std dev 0.60 mm). In the US image, these correspond to a reconstructed error per direction of 3.12 pixels (max 8.42 pixels) and 7.66 pixels (max 18.22 pixels) in x- and y-direction respectively. The optimized parameters were verified with 7 points not used for optimization. Verification terminated with an average error of 0.78 mm (max 1.74 mm, std dev 0.51 mm) , see Fig.12. In the image, these correspond to a reconstructed error per direction of 1.42 pixels (max 3.60 pixels) and 5.77 pixels (max 12.86 pixels) in x- and y-direction respectively.

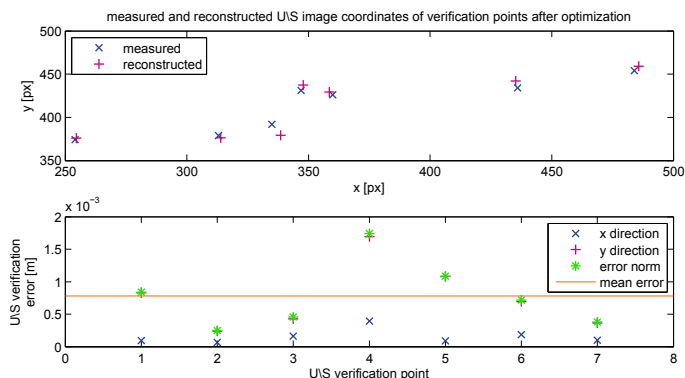


Fig. 12 Parameter verification for ultrasound probe calibration.

3.3 X-ray image Registration

Since the robot is not localized with respect to the mammography device, a registration step is necessary to obtain the transformation matrix between \mathcal{F}_0 and \mathcal{F}_X . The chosen method relies on measuring the coordinates of reference points in both the robot and x-ray image space. The registration tool is a nylon plate containing 15 lead ball bearings (BBs) which was positioned on top of the breast phantom. Fiducial markers have been randomly placed on a plate covering the entire breast phantom surface. The markers are 1 mm diameter BBs highly visible in x-ray images. An x-ray scan of the registration plate is performed. The BBs coordinates are determined in the x-ray images. To obtain the coordinates of the target points in the robot space, a localization tip was used. Each target point coordinates w.r.t. the robot base are computed thanks to DH parameters identified in Sec.3.1 and to a tool model.

The registration points on the nylon paddle are determined in the robot base by manually pointing on them using the robot equipped with the calibrated tool (see Fig.13). During this phase, the robot is controlled to apply a null force and it can be easily moved thanks to its high backdrivability. The obtained coordinates are then mapped to the point coordinates determined in the MX images. This mapping is done using an iterative closest point algorithm (ICP), [2].

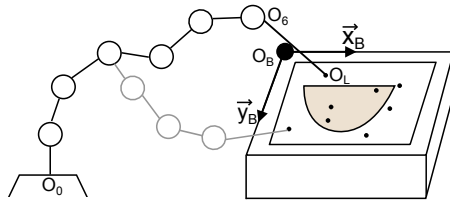


Fig. 13 Geometrical model for x-ray image registration.

Nine marker coordinates are used to optimize the transformation parameters. The remaining five points are used to verify the optimization algorithms and to confirm the error. The chosen target points for optimization and validation are distributed all over the registration plate. The ICP algorithm terminates with an average error of 0.70 mm (max 1.06 mm, std dev 0.24 mm). The optimized parameters were verified with 5 points, giving an average error of 0.73 mm (max 1.59 mm, std 0.48 mm), see Fig.14.

3.4 Total Setup Error

To estimate the final set-up error, six target points (lesion GC of the anatomic phantom) were chosen. Their coordinates were determined in the x-ray and US images. For the latter ones, the US-probe was positioned manually. After successful calibration of each system component, both independent ways to measure the same target point should give the same result. A difference between both measures indicates a

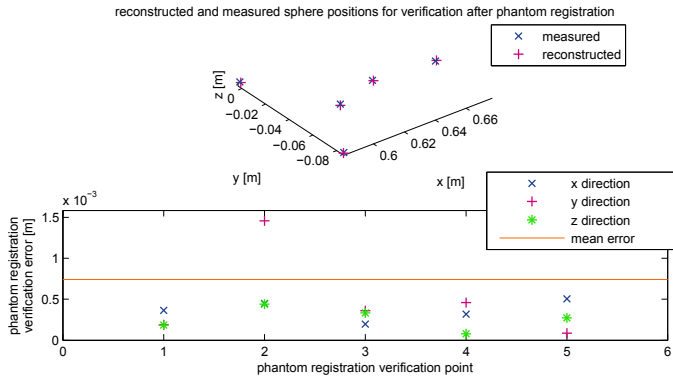


Fig. 14 X-ray image to robot verification.

calibration/registration error of the system. Thus, the GC were measured in \mathcal{F}_P and \mathcal{F}_X separately. To estimate the error between both sets, they were expressed in \mathcal{F}_P . The transformation from \mathcal{F}_X to \mathcal{F}_P is possible thanks to the previous calibration steps. Indeed, any point $Q_X|_X$ expressed in \mathcal{F}_X can be expressed in \mathcal{F}_P by:

$$Q_X|_P = M_{PX} Q_X|_X = M_{P6} M_{60} M_{0X} Q_X|_X \quad (1)$$

Target points have been identified in the breast phantom to estimate the total setup error. The point coordinates have been determined in the x-ray images, Q_X in Fig.15. The same target points have been visualized using US and are denoted Q_P . Thanks to the previous probe to end-effector calibration, the distance between Q_X and the US-beam could be calculated:

$$d_z = |(Q_X - Q_P)^T \mathbf{z}_P| \quad (2)$$

The average distance between the GC measured in x-ray images and the US beam is

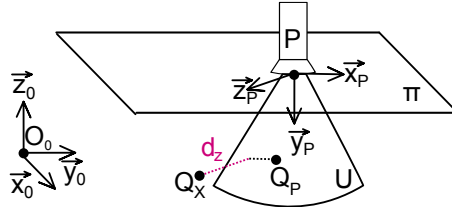


Fig. 15 Geometrical model total set-up error.

1.29 mm (max 2.23 mm, std 0.84 mm), see Fig.16. Note, that this estimation depends on the manual position capabilities. A human error is thus induced in this procedure. Nevertheless, the US-probe was positioned by a user who already knew the breast phantom while paying much attention. The total set-up error is due to the following identified possible sources of error:

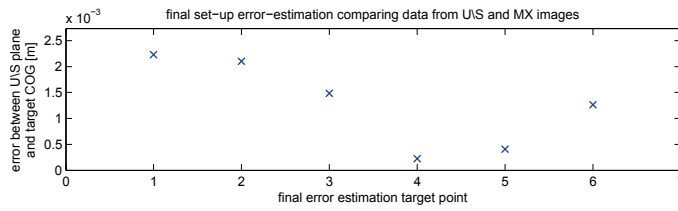


Fig. 16 Total set-up error.

- the robot internal position error,
- the BBs used for registration and their diameter of 1 mm,
- the reconstruction distance of 0.5 mm between the x-ray image slices (relatively low resolution),
- the localization-tip diameter of 0.25 mm,

Taking into account the medical context in which this system would be used, the total error looks pretty acceptable. Indeed, the smallest lesions detected in clinical practice with US are about 5 mm in diameter.

4 Robot Control

Robot-assisted US examination of BC detection can be modeled as a pointing / scanning task where the user is assisted by a robot, who knows the location of the lesion. Since the breast remains compressed after MX, the US scan is to be performed through the compression paddle. The radiologist's task is to find and scan the suspicious zone while maintaining contact between the probe and the paddle. For better visibility, physicians often display the lesion in the middle of the US image, on its main axis. The task of a conventional US scan has a total of 6 DOFs. However, it can

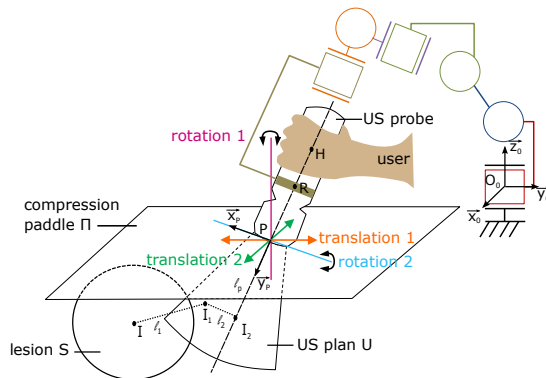


Fig. 17 DOF of a US scan of a compressed breast through a rigid compression paddle.

be reduced to a 4-DOFs task at the probe-tip thanks to the assumption of constant

probe-paddle contact. Two movements would lead to a loss of probe-paddle contact and thus are not part of the task:

- translations along the paddle normal vector,
- rotations around vector normal to the US beam.

The positioning task possesses thus 4 DOF, as shown in Fig.17: two translations of the probe-tip on the paddle, assumed to be planar, one rotation along the normal vector of the paddle surface, and a second rotation around the intersection line of the paddle-surface and the US-plane. Even if the task is associated with scanning, i.e. the full coverage of a region of interest (ROI), this can be reduced to a pointing task based on the hypothesis of a moving point of interest (POI) within the ROI. The compression paddle is associated with a plane π while the ultrasound beam plane is denoted U . In the next, the following notations are used:

- The US-probe is handled by the user at point H on the US-probe main axis.
- The robot wrench is applied on the probe at point R on the US-probe main axis.
- The central point of the suspicious lesion S is denoted I and its projection on U is denoted I_1 with $I_1 - I = l_1 \mathbf{z}_P$.
- The projection of I on the US-probe main axis is denoted I_2 , $I_2 - I_1 = l_2 \mathbf{x}_P$.

The task consists of centering the suspicious lesion in the image, which is hence divided into two parts:

1. assuring intersection between the US-plane and the lesion ($I = I_1$),
2. centering the lesion in the image ($I_1 = I_2$).

As stated in Sec.1, it is important to allow imaging tissues surrounding the lesion, as well as letting the radiologist to choose the probe orientation in order to avoid undesired shadows and to observe the lesion from a desired angle of view. Consequently, the robot should not completely prevent the user from moving away from the target. To simulate such behavior, a robot control that generates a wrench corresponding to the sum of two compression springs of stiffness, k_1 and k_2 respectively, was implemented. Both springs have a null free length. One connects I and I_1 whereas the second one connects I_1 and I_2 :

$$\mathcal{E}_1 = [0 \ 0 \ -k_1 l_1 \ 0 \ 0 \ 0]^T_{I_1} ; \quad \mathcal{E}_2 = [-k_2 l_2 \ 0 \ 0 \ 0 \ 0 \ 0]^T_{I_2} \quad (3)$$

The applied wrenches thus provide a state of equilibrium at $I = I_1$ and $I_1 = I_2$, when the task is successfully accomplished. The complete wrench applied to execute the task is the sum of \mathcal{E}_1 and \mathcal{E}_2 :

$$\mathcal{E}_{task} = \mathcal{E}_1 + \mathcal{E}_2 \quad (4)$$

$$= [-k_2 l_2 \ 0 \ -k_1 l_1 \ -k_1 l_1 l_P \ -k_1 l_1 l_2 \ k_2 l_2 l_P]^T_P \text{ with } (I_2 - P) = l_P \mathbf{y}_P. \quad (5)$$

This controller is applied to the robot at a 1kHz rate. In order to ease the manipulation, a viscosity term depending on the end-effector velocity at O_6 is added for proper damping, while a gravity compensation of the US probe's weight is added.

5 Experiments

5.1 Protocol

Tests have been performed by 22 naive subjects using the setup. A large number of subjects has been recruited to account for inter-subject variability and still obtain statistically significant results. It was not possible to recruit such a large number of radiologists. This is why the results are not to be considered as an absolute performance evaluation but, rather, as a differential comparison between assisted and non-assisted manipulation. Notice that since the task to be realized is not a conventional clinical gesture, even radiologists would have been considered as naive subjects with respect to the task and the robot assistance.

For Test 1, the subjects are presented with a target lesion chosen in the MX images. They start (at $t = 0$) with the US-probe in its rest position (at one corner of the breast phantom) and have to localize this particular target on the phantom using US. When subjects think they have localized the lesion from a first guess, they give a vocal feedback (at $t = t_1$). Then, they proceed to analyze the surrounding tissues (seeking for other points of interest) in order to verify their first guess, as a radiologist would do in a real situation. Once they are certain to have localized the lesion, a second vocal feedback is given (at $t = t_2$) and the test is stopped. During Test 2, the subjects are asked to scan the entire target lesion (not only its central point) using US. This corresponds to a clinical phase where the radiologist wants to characterize the lesion (shape and size). Test 2 starts (at $t = t_3$) with the US-probe already positioned above the lesion to be examined. Four different scanning methods are used within Test 2. First, the user is asked to visualize the lesion in the US images under as many different perspectives (probe orientations) as possible within 30 sec. For the three remaining scanning methods, the subject is asked to execute a particular movement and has only 10 sec to scan the lesion. Three movements compatible with the probe-paddle contact geometry are selected: translations along the compression paddle plane, rotations around the paddle normal vector \mathbf{n}_π and rotations around the intersection of the US-plane and the paddle surface ($\mathbf{z}_P \times \mathbf{n}_\pi$). Test 2 terminates at $t = t_e$. The two tests performed are summarized here, see Fig. 18:

- Test 1: subtask one and two: approximate target localization followed by proper target identification.
- Test 2: subtask three: entire target lesion-scan.

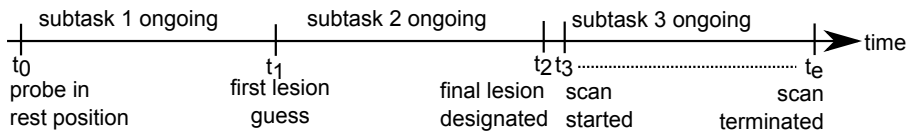


Fig. 18 Time line for Tests.

The tests are run under two conditions: either the robot is in a transparent mode (no forces applied, mode 1) or the robot applies the elastic force fields depicted in

Sec.4 (mode 2). To avoid increasing learning effects, all tests 1 (for both actuation modes) have been executed in a row and prior to tests 2. The subjects have thus not been habituated to the phantom geometry during tests 1. User performances for each mode were compared. For tests 1, two performance indicators were chosen:

- US plane-to-target distance (precision), $d_z = \text{mean}(|(I - I_1)^T \mathbf{z}_P|)$,
- completion time (duration), t_2 .

In order to compare the different time performances, they were normalized over the entire duration of the series of tests 1 for each subject and both actuation modes, e.g.

$$\text{for mode } i: t_{l,i} = \frac{t_{2,i} - t_{0,i}}{\sum_1^2 (t_{2,i} - t_{0,i})}.$$

Results of tests 2 have been grouped for each actuation mode, independent of the movement. The performance indicators are:

- The visibility ratio t_s defined as the ratio between the time span when US-plane U and lesion volume S intersect (*i.e.* when the lesion is visible) and the total duration of the scanning test: $t_s = \frac{t'_s}{t_e - t_2}$, with $t'_s = \sum_{t_2}^{t_e} (t_i - t_{i-1}), \forall t_i \in \{t_3, \dots, t_e\} : (S \cup U)$ and $t_e - t_2 = 30\text{s}$ as imposed by the protocol.
- the US plane-to-target distances (precision), $d_z = \text{mean}(|(I - I_1)^T \mathbf{z}_P|)$,

Test data has been analyzed using statistical ANOVA (analysis of variance) tests. It indicates whether or not the results obtained per control mode are significantly different. The result of ANOVA tests gives so-called p- and F-values which have to be interpreted w.r.t. level of confidence as shown here:

- the F-value is the ratio of the variance *between* control modes and the variance *within* each control mode. It quantifies the separation of each sampling group (here control mode) w.r.t. the others. The higher the F-value, the more the samplings (control mode) are significantly different.
- the p-value depends on the actual F-value. A low p-value indicates a high confidence in the given statistical result. For a low p-value, it is highly probable that the control modes have significant influence on user performances.

In case of $p < 0.05$, one can conclude that the robot control modes have altered the effects on user performances in relation to the analyzed data to a significance level of 95%.

5.2 Results

Table 1 shows the number of properly located lesions for each control mode at the end of Tests 1.

Table 2 shows how subjects changed their guess between the first and second feedback. Without guidance, two subjects rectified their first guess and one finally chose a wrong lesion as target although it was properly localized at the first feedback. One subject rectified his initial guess with assistance, in a positive way.

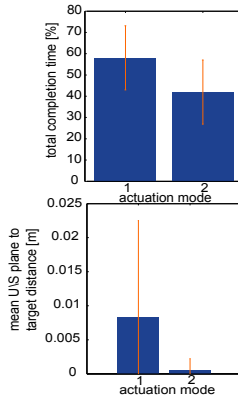
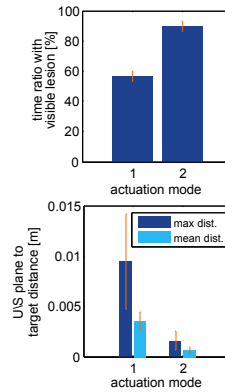
Table 1 Number of properly located lesions during Tests 1 over 22 subjects

actuation mode	1 (without guidance)	2 (with guidance)
Results at $t = t_1$	12	14
Results at $t = t_2$	13	15

Table 2 Change of chosen lesion between both feedbacks during test 1

actuation mode	1 (without guidance)	2 (with guidance)
wrong \rightarrow proper	2	1
proper \rightarrow wrong	1	0
no change, wrong	8	7
no change, proper	11	14

Indicators for tests 1 averaged across subjects are plotted in Fig.19. The average normalized time needed to localize the lesion was longer in mode 1 ($\bar{t}_{l,1} = 58.1\%$, $\sigma=15.1\%$) than in mode 2 ($\bar{t}_{l,2} = 42.0\%$, $\sigma=15.1\%$), which represents a 28.0% time reduction brought by the robot guidance. Users also performed worst with mode 1 regarding precision. In this mode, the average US plane-to-target distance, (\bar{d}_z) is 0.8 cm (1.43 cm), while it is only 0.05 cm (0.17 cm) in mode 2. This represents an improvement of 94.0% brought by robot guidance. This accuracy can be considered sufficient to image lesions of 0.5 cm diameter in practice.

**Fig. 19** Results of Tests 1: mean localization time and US plane-to-target distance.**Fig. 20** Results of Tests 2: results for visibility ratio and US plane-to-target distance.

One factor ANOVA with subjects as repeated measures was used to analyse each indicators. The robot guidance has a significant effect on the US plane-to-target distances ($F = 7.2$ and $p = 0.014$). Results of completion time ($F = 6.3$ and $p = 0.020$) showed a less but still significant effect for the experiment conditions. Indicators for Test 2 are plotted in Fig.20. With mode 1, the visibility ratio \bar{t}_s averaged across sub-

jects was 56.7% (std dev 3.3%) of the total duration of Tests 2. Users have thus only spent about half of the time imaging the lesion, the rest of the time, it was not visible in the US images although they were explicitly asked to maintain visibility during the scanning movement. With mode 2, \bar{t}_s reached 89.8% (std dev 3.4%). The target to plane distance averaged across subjects, \bar{d}_z was analyzed regarding its mean and maximum values across the four different scanning methods of Tests 2, denoted $\text{mean}(\bar{d}_z)$ and $\text{max}(\bar{d}_z)$ respectively. The indicator $\text{max}(\text{mean}(d_z))$ is larger in mode 1 (0.95 cm (std dev 0.47 cm)), to be compared to 0.16 cm (std dev 0.1 cm) for mode 2. The maximal distance was thus decreased by 83% by the use of guidance. A similar relation can be observed for $\text{mean}(\bar{d}_z)$. Its value is 0.35 cm (std dev 0.09 cm) for mode 1 and only 0.06 cm (std dev 0.03 cm) for mode 2. This corresponds to an improvement of 82%. One factor ANOVA run with subjects as repeated measures again showed a significant effect of the two actuation modes: $F = 210.8$, $p = 0.0007$ for visibility ratio, $F = 17.2$, $p = 0.0250$ for max US-plane to target distance and $F = 80.2$, $p = 0.003$ for mean US plane-to-target distance. P-values are equally below 0.002 for results of each independent tests 2 series (i.e. free movement or the three imposed movements).

6 Discussion and conclusion

The aim of this work was to propose a solution for combining MX and US breast-scans without changing the breast geometry. This is motivated by clinical literature reporting diagnostic errors due to breast geometry changes between MX and US examinations. In order to minimize the dual-examination duration, which is crucial as breast compression induces pain to the patient, we have proposed to assist the physician in locating, with the US probe, a lesion identified in the 3D MX images. A comanipulated robot was developed to help scanning the breast with an US probe through the MX compression paddle.

In order to allow for immediate operation as soon as the patient is installed, we have proposed to install the robot fixed w.r.t. the DBT imaging device and to calibrate the system. The over-all system precision is 1.29 mm which is sufficient with regard to the clinical application, where lesions of 5 mm need to be identified.

A test protocol was presented to conduct two tests that are both related to the medical application. The first tests aims at evaluating robot guidance for localizing a lesion which was previously defined in the X-ray images. The second tests aims at quantifying robot influence when scanning a target lesion. The studied task consists of a pointing/scanning exercise, where the US beam intersects a breast lesion.

Table 1 shows a slight increase in the ability of properly identifying the target lesion thanks to the use of the robot. The low stiffness used throughout the experiments in order to let the user scan the system is certainly a reason for that low improvement, which is yet of approx. 10%. More importantly, the use of a robot increases precision during both tests, nearly 94%. Furthermore, it decreases the time needed to properly localize a target using US by nearly 30%. During the scanning phase, the visibility ratio was increased by 60%, indicating that keeping the lesion visible during the US scanning phase is easier. We hypothesize that this could allow for localizing smaller lesions.

In summary, it was shown that user performance increased significantly with robot assistance in terms of speed and precision.

Conflict of interest : This work is partially funded by ANRT under CIFRE grant 247/2009 and by french state funds managed by the ANR within the Investissements d’Avenir programme (Labex CAMI) under reference ANR-11-LABX-0004. The authors declare that they have no conflict of interest.

Research involving human participants: All procedures performed in studies involving human participants were in accordance with the ethical standards of the institutional and/or national research committee and with the 1964 Helsinki declaration and its later amendments or comparable ethical standards.

This article does not contain any studies with animals performed by any of the authors.

Informed consent: Informed consent was obtained from all individual participants included in the study.

References

1. Berg, W.A., Blume, J.D., Cormack, J.B., Mendelson, E.B., Lehrer, D., Bhm-Vlez, M., Pisano, E.D., Jong, R.A., Evans, W.P., Morton, M.J., Mahoney, M.C., Hovanesian Larsen, L., Barr, R.G., Farria, D.M., Marques, H.S., Boparai, K.: Combined screening with ultrasound and mammography vs mammography alone in women at elevated risk of breast cancer. *The Journal of the American Medical Association (JAMA)* **299**(18), 2151–2163 (2008)
2. Besl, P.J., McKay, H.D.: A method for registration of 3-d shapes. *IEEE Transactions on Pattern Analysis and Machine* pp. 227–241 (1992)
3. Bonneau, E., Taha, F., Gravez, P., Lamy, S.: Surgicobot: Surgical gesture assistance cobot for maxillo-facial interventions. *Perspectives in Image-Guided Surgery* pp. 353–360 (2004)
4. Booi, R.C., Kruecher, J.F., Goodsitt, M.M., O’Donnell, M., Kapur, A., LeCarpentier, G.L., Roubidoux, M.A., Fowlkes, J.B., Carson, P.L.: Evaluating thin compression paddles for mammographically compatible ultrasound. *Ultrasound in Medicine & Biology* **33**(3), 472–482 (2007)
5. Buchberger, W., Niehoff, A., Obrist, P., DeKoekkoek-Doll, P., Duenser, M.: Clinically and mammographically occult breast lesions: detection and classification with high-resolution sonography. *Seminars in Ultrasound, CT and MRI* **21**(4), 325–336 (2000)
6. Conway, W., Hayes, C., Brewer, W.: Occult breast masses: use of a mammographic localizing grid for us evaluation. *Radiology* **181**(1), 143–146 (1991)
7. Davies, B., Fan, K., Hibberd, R., Jakopec, M., Harris, S.: A mechatronic based robotic system for knee surgery. *IASTED International Conference on Intelligent Information Systems* pp. 48–52 (1997)
8. Dombre, E., Khalil, W.: *Robot Manipulators: Modeling, Performance Analysis and Control*. Control Systems, Robotics and Manufacturing Series (2007)
9. D’Orsi, C., Bassett, L., Berg, W.: *Breast Imaging Reporting and Data System: ACR BI-RADS-Mammography*, 4 edn. Reston, VA, American College of Radiology (2003)
10. Francoise, V., Sahbani, A., Morel, G.: A comanipulation device for orthopedic surgery that generates geometrical constraints with real-time registration on moving bones. In: *Robotics and Biomimetics (ROBIO)*, 2011 IEEE International Conference on, pp. 38–43 (2011)
11. Gordon, P., Goldenberg, S.: Malignant breast masses detected only by ultrasound: a retrospective review. *Cancer* **76**(4), 626–630 (1995)
12. Harvey, J.A., Bovbjerg, V.E.: Quantitative assessment of mammographic breast density: Relationship with breast cancer risk. *Radiology* **230**(1), 29–41 (2004)
13. Kaplan, S.: Clinical utility of bilateral whole breast us in the evaluation of women with dense breast tissue. *Radiology* **221**(3), 641–649 (2001)

14. Kapur, A., Carson, P., Eberhard, J., Goodsitt, M., Thomenius, K., Lokhandwalla, M., Buckley, D., Roubidoux, M., Helvie, M., Booi, R., LeCarpentier, G., Erkamp, R., Chan, H., Fowlkes, J., Thomas, J., Landberg, C.: Combination of digital mammography with semi-automated 3d breast ultrasound. *Technology in cancer research & treatment* **3**(4), 325–334 (2004)
15. Kolb, T.M., Lichy, J., Newhouse, J.H.: Comparison of the performance of screening mammography, physical examination, and breast us and evaluation of factors that influence them: An analysis of 27,825 patient evaluations¹. *Radiology* **225**(1), 165–175 (2002)
16. Kragic, D., Marayong, P., Li, M., Okamura, A.M., Hager, G.D.: Human-Machine Collaborative Systems for Microsurgical Applications. *The International Journal of Robotics Research* **24**(9), 731–741 (2005)
17. Leconte, I., Feger, C., Galant, C., Berlire, M., Berg, B., D’Hoore, W., Maldague, B.: Mammography and subsequent whole-breast sonography of nonpalpable breast cancers: the importance of radiologic breast density. *American Journal of Roentgenology* **180**(6), 1675–1679 (2003)
18. Poquet, C., Vitrani, M.A., Morel, G.: Proximal comanipulation of a minimally invasive surgery instrument to emulate distal forces. In: CRAS 2014, 4th Joint Workshop on New Technologies for Computer/Robot Assisted Surgery, pp. 48–51 (2014)
19. Schneider, O., Troccaz, J.: A six degree of freedom passive arm with dynamic constraints (padyc) for cardiac surgery application: Preliminary experiments. *Computer-Aided Surgery, special issue on medical robotics* **6**, 340–351 (2001)
20. Schneider, O., Troccaz, J., Chavanon, O., Blin, D.: Padyc: a synergistic robot for cardiac puncturing. *IEEE International Conference on Robotics and Automation(ICRA)* pp. 2883–2888 (2000)
21. Vitrani, M.A., Morel, G.: Hand-eye self-calibration of an ultrasound image-based robotic system. *IEEE/RSJ International Conference on Intelligent Robots and Systems (IROS)* pp. 1179–1185 (2008)